Received: 24 October 2022 | Revised: 9 December 2022 | Accepted: 13 December 2022

DOI: 10.1002/esp.5527

RESEARCH ARTICLE

ESPL WILEY

Slope stability evolution of a deep-seated landslide considering a constantly deforming topography

Jan Pfeiffer[1,2] | Thomas Zieher[1,2] | Barbara Schneider-Muntau[3]

[1]Institute for Interdisciplinary Mountain Research, Austrian Academy of Sciences, Innsbruck, Austria

[2]Department of Geography, University of Innsbruck, Innsbruck, Austria

[3]Department of Infrastructure Engineering, University of Innsbruck, Innsbruck, Austria

Correspondence
Jan Pfeiffer, Institute for Interdisciplinary Mountain Research, Austrian Academy of Sciences, Innrain 25, 6020 Innsbruck, Austria.
Email: jan.pfeiffer@oeaw.ac.at

Funding information
Horizon 2020 Framework Programme, Grant/Award Number: 776848

Abstract

Slow-moving deep-seated landslides are characterised by continuous deformation, constantly changing topography and sliding-mass geometry. Deformation rates are predominantly controlled by temporal dynamics of pore pressure. Progressing movements typically cause an over-steepening of a landslide's foot, making these areas more susceptible to secondary slope failures and piggyback slides that, once they occur, change the geometric boundary conditions of a slope. This study presents an integrated topographic monitoring and geomechanical modelling approach, which is suitable for both model-based replication of the landslide's hydro-meteorological drivers and assessment of the long-term effect of topographic changes on the stability behaviour of a large deep-seated landslide. Parametrised at the Vögelsberg landslide (Tyrol, Austria) the integrated approach quantified considerable mass relocations between 2007 and 2020 at the landslide's foot and assessed respective effects on slope stability. Additionally, scenarios of past and future topographies were reconstructed and projected. Mass relocations of the order of 25 000 m^3 were assessed between multiple airborne laser scanning acquisitions covering a period of 13 years. Based on annual uncrewed aerial vehicle laser scanning campaigns, area-wide 3D displacements were analysed, exceeding a magnitude of 200 cm a^{-1} at small parts (2.500 m^2) on the steeper foot of the active landslide. The main landslide body (0.28 km^2) moves considerably slower with movements of 2–10 cm a^{-1}. Besides spatio-temporally varying hydrological drivers, topographic changes can have a severe impact on slope stability and therefore modify the spatiotemporal activity of the landslide. It is shown that, besides the hydrometeorological drivers, the varying elevation of the landslide's toe is a key parameter determining the long-term trend of slope stability. With the presented approach the formation and evolution of the Vögelsberg landslide can be understood and explained.

KEYWORDS
deep-seated landslide, geomechanical modelling, landslides, laser scanning, OPERANDUM, slope stability, topography

1 | INTRODUCTION

Slowly deforming slopes in mountainous areas are a widespread phenomenon, continuously changing topography by complex and nested spatio-temporal activity patterns (Crosta et al., 2013). These processes are referred to as deep-seated gravitational slope deformations (DSGSDs), where spatial and temporal varying displacements of several millimetres up to a few centimetres per year are typically observed (Ambrosi & Crosta, 2006; Brckl et al., 2006). They promote the formation of deep-seated landslides as subunits, with displacements exceeding 1 m per year (Lacroix et al., 2020; Pfeiffer et al., 2018). Shear zones or sliding surfaces can evolve hundreds of metres

below the surface, whereas complex internal deformation structures contribute to a uniquely and constantly changing slope geometry. Characteristic geomorphological features are scarps, trenches, grabens and double or multiple crested ridges in the upper parts, counter-scarps in the slope's mid-section and bulging, buckling folds and highly fractured rock masses at the slope's foot (Agliardi et al., 2012; Chigira, 1992; Crosta et al., 2013). Besides their characteristic landscape-shaping behaviour, slow deformations can cause serious damage to infrastructure and affect livelihoods. In order to prevent damage and mitigate the hazard, detailed knowledge of the hydromechanical factors controlling the sliding behaviour is of great relevance (Bonzanigo et al., 2007; Eberhardt et al., 2007; Hofmann & Sausgruber, 2017).

Once a DSGSD has developed by strain localisation and consequential formation of shear zones (Agliardi et al., 2013; Zangerl et al., 2010, 2015), the activity of therein hosted deep-seated landslides is generally controlled by changes in the stress fields (Eberhardt, 2008; Preisig et al., 2016). Predominantly, these changes are induced by fluctuations in pore-water pressure (PWP) and accompanying changes in effective stress in a landslide's shear zone. Several studies have demonstrated the correlation between PWP or groundwater-related variables (e.g., groundwater recharge, reservoir level) with landslide activity (Bonzanigo et al., 2007; Eberhardt et al., 2007; Zangerl et al., 2010). Changes in PWP typically occur within short time periods, leading to seasonal or episodic phases of accelerated landslide movement after prolonged rainfall and intense snowmelt (Pfeiffer et al., 2021). Over longer periods, nested slope deformations (DSGSDs) cause significant topographic changes, leading to an over-steepening of the foot. Once a critical threshold of over-steepening is reached, secondary and spontaneous slope failures are commonly observable phenomena (Agliardi et al., 2012; Glueer et al., 2019). These short-term mass relocation processes, on the other hand, induce stress and strain relocation, which may also affect the activity of the DSGSD or enclosed deep-seated landslides. Continuous deformation degrades the rock strength by fracturing, fragmentation and alteration (Preisig et al., 2016). The longer the deformation, the more intense is the strength degradation. In this context, secondary slope failure processes at the continuously steepening and degrading foot evolve to be increasingly likely. Buttressing effects by interactions of the landslide's toe with the alluvium of a dynamic river bed additionally influence the slope's geomechanical conditions (Zangerl et al., 2015).

Several studies aim at reproducing the activity of hydrometeorologically driven deep-seated landslides using a variety of model approaches. Van Asch and Buma (1997) developed a hydrological model to describe groundwater fluctuations and their impact on the temporal frequency of instability of landslides. Corominas et al. (2005) proved that prediction of landslide displacements from groundwater level is feasible by rheological parameters and solving the momentum equation extended by a viscous term (Bingham and power law). Preisig (2020) exploited a one-way coupled hydromechanical numerical modelling strategy to assess slope stability under expected groundwater pressure changes. Whereas the hydrological component is well represented by a large number of studies (Corominas et al., 2005; Preisig, 2020; Van Asch & Buma, 1997), the geomechanical effect of changing slope geometries is only marginally investigated in the existing literature and predominantly based on theoretical assumptions (Molnar, 2004). In particular, the lack of accurate topographic long-term monitoring data is supposed to be a key issue for a precise reassessment of historic, past, or even pre-failure slope stability conditions. Zangerl et al. (2015, 2021) respond to these challenges by reconstructing pre-failure topographies based on present-day digital terrain models (DTMs) combined with the interpretation of the landslide's geomorphological features.

Recently, precise and detailed assessments of landslide topographies can be performed with the help of various remote sensing technologies. Laser scanning and photogrammetry performed from different platforms provide crucial topographic data for investigating a variety of landslide-associated research questions (Gigli et al., 2014; Jaboyedoff et al., 2012; Scaioni et al., 2014). Different sensor and acquisition methods acquiring 3D surface data induce a multitude of advantages, disadvantages and challenges depending on the research's aim (Salvini et al., 2013; Scaioni et al., 2014; Tofani et al., 2013). Whereas passive photogrammetric methods face challenges in densely vegetated areas, laser scanning as an active remote sensing technique is feasible for retrieving topographic data, even below the canopy (Baltsavias, 1999). Hence multitemporal airborne laser scanning (ALS) acquisitions represent an important and ready-to-use data archive. Complemented by more accurate, temporally and spatially higher resolved uncrewed aerial vehicle laser scanning (ULS) campaigns, solid time series of topographic 3D data can be made available (Zieher et al., 2019). These datasets provide a unique archive to investigate landslide-induced topographic changes well suited to be integrated in any geomechanical modelling framework of a deep-seated landslide.

Here we present a geomechanical modelling strategy that is able to assess and replicate the activity of a subunit of a large DSGSD—the Vögelsberg landslide (Tyrol, Austria; for location see Figure 1b,d)—under different hydrological and topographic conditions. Changes in the model's geometry are precisely assessed using combined ULS and ALS data covering a period of 13 years. Thus, geomorphological processes responsible for assessed topographic changes are identified and quantified. Based on these precise observations, potential future topographic scenarios and a pre-failure topography were approximated and discussed. Geomechanical modelling was carried out for both different hydrological and topographic parametrisations. Objectives of the present study were to

- assess recent topographic changes, reconstruct a probable pre-failure topography and project potential future topographic conditions of the Vögelsberg landslide,
- parametrise a slope stability model accounting for both changing topographic and hydrological boundary conditions,
- present and quantify the impacts of long-term topographic changes and seasonal hydrological conditions on the landslide activity, and
- identify and quantify critical parameters controlling the evolution and formation of the Vögelsberg landslide.

2 | STUDY AREA

The northeastern-facing slope at the entrance of the Watten valley from 750 to 2200 m a.s.l. is subject to a large DSGSD (Figure 1b).

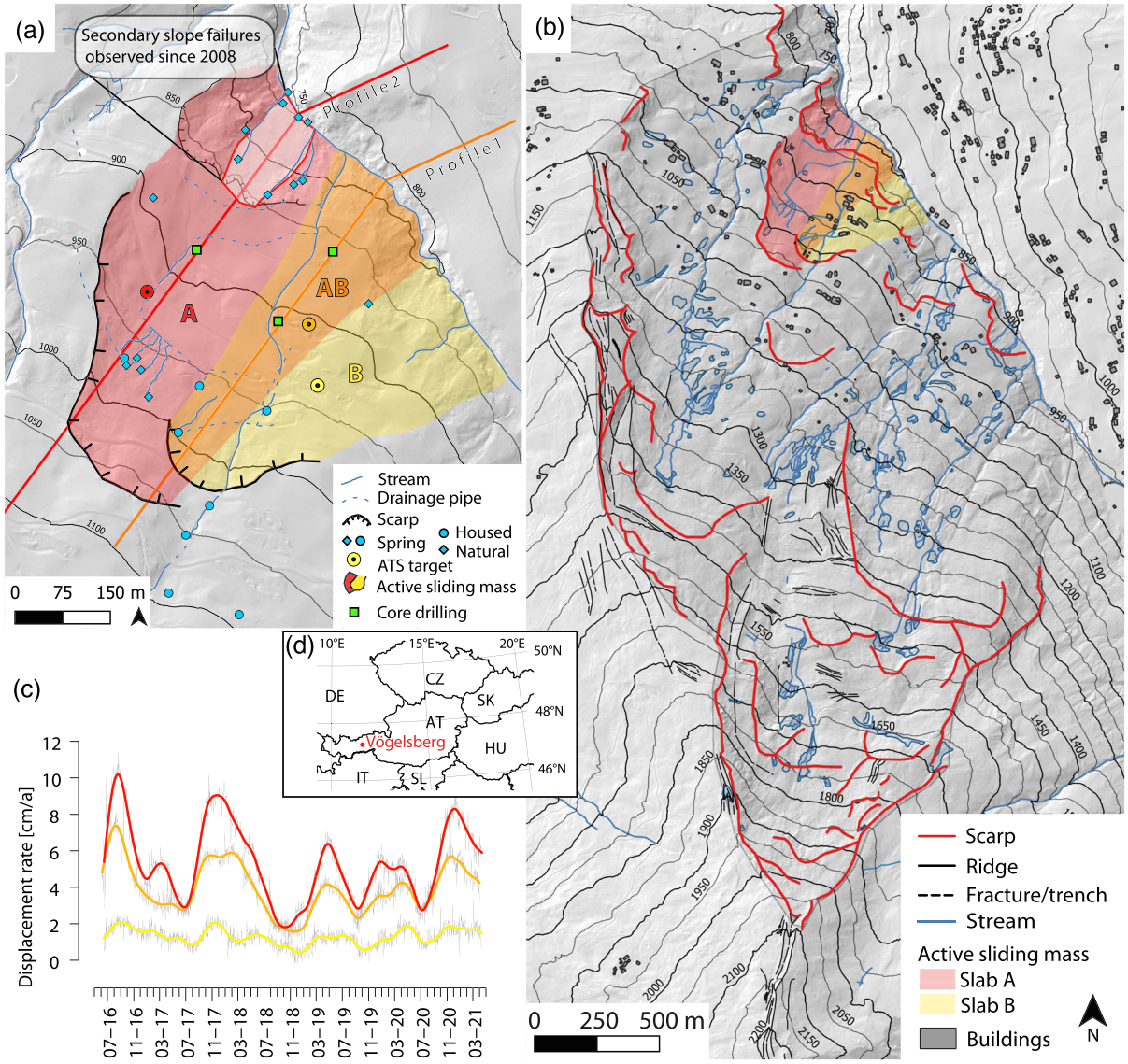

FIGURE 1 Overview of the active part of the Vögelsberg landslide. (a) Detailed map of the sliding area, position of selected ATTS reflectors, core drilling and springs (sliding mass division, after Engl, 2018). (b) Map showing morphological structures and outline of the DSGSD. (c) Time series of displacement rate at selected ATTS reflectors and (d) location of the Vögelsberg landslide (data source DTM and ATTS: Federal State of Tyrol) [Color figure can be viewed at wileyonlinelibrary.com]

Located within the Lower Austroalpine Innsbruck Quartzphyllite complex (Haditsch & Mostler, 1983; Rockenschaub et al., 2003), varieties of quartzphyllite characterise the geological setting of the DSGSD. An active sliding mass (i.e., deep-seated Vögelsberg landslide) is situated on the foot of the DSGSD. Here, two varieties of quartzphyllite are noticeable: in the hanging a quartz-rich sericite phyllite containing metacarbonatic intercalations and in the lying a chlorite–sericite–phyllite (Engl, 2018). Prominent, narrow and isoclinal folded schistosity slightly dipping towards WNW is apparent at outcrops around the DSGSD (Pfeiffer et al., 2022). A high degree of fragmentation and decomposition can be recognised at the Vögelsberg landslide's foot. (Engl, 2018).

The bulged and compressed toe at the Wattenbach and the extensionally imprinted ridge in the upper and southernmost part of the study area indicate complex, large-scale and deep-seated slope deformations covering an area of approximately 4 km^2. These morphological features of deep-seated and nested slope deformations overprint a glacially shaped valley morphology and hence provide evidence for post-glacial deformation activities. Situated between 750 and 1050 m a.s.l., the Vögelsberg landslide is known to cause damage to buildings and infrastructure (Zieher et al., 2019). The Vögelsberg landslide covers an area of approximately 0.28 km^2 and is subdivided into two interacting slabs based on morphological indications (Figure 1a; (Engl, 2018)). The higher lying crown of the northwestern slab (Slab A), as well as its very pronounced bowl-shaped central part, indicate a more intense deformation history compared to the southeastern slab (Slab B). Recent automated tracking total station (ATTS) measurements prove this observation and show the highest (up to 10 cm a^{-1}) and most dynamic velocity on a reflector target situated on slab A (Figure 1c). An ATTS target mounted in the intersection zone (Slab AB) of the two slabs shows smaller (up to 7 cm a^{-1}) but still temporally varying velocity. In contrast, an ATTS target mounted on Slab B shows almost constant velocity of 2 cm a^{-1} without distinct temporal variations.

As a consequence of intense precipitation in October 2008, the foot of the over-steepened Vögelsberg landslide failed with a lateral extent of up to 100 m and failure depths of multiple metres (Klebinder & Graf, 2012). The onset of this slope failure occurred at an elevation of 860 m a.s.l., which simultaneously marks a prominent change in the slope's gradient. Whereas a steeper slope towards the Watten River is located below the onset of failure, a moderately inclined slope characterises the area above and is assumed to result from combined deep-seated slope deformation and glacial overprinting. In spring 2009, this piggyback landslide slowed down but episodically reactivated after distinct precipitation events. Overall, it can be assumed that this secondary process has relocated a significant amount of material and therefore explicitly modified the topography of the Vögelsberg landslide. The nearby Wattenbach, draining an approx. 73 km^2 big catchment, has shown significant fluvial and torrential activity during the Holocene (Patzelt, 1987). Fluviatile influence at the Vögelsberg could be mapped from the recent Watten River elevation (ca. 750 m a.s.l.) to the change in the slope's gradient and onset of recent spontaneous slope failures at 860 m a.s.l. Moreover, recent fluvial dynamics were observed to play a crucial role in the context of the secondary failure processes on the foot of the Vögelsberg landslide (Grafenauer, 2014).

3 | MATERIALS AND METHODS

3.1 | Modelling strategy and background

In order to assess and replicate the geomechanical behaviour of the Vögelsberg landslide under changing hydrological and topographic conditions (Figure 2), a reproducible and purpose-fitting strategy of model parametrisation was established based on following background assumptions. As conceptualised in Figure 2, multiple geomorphological processes are known to shape a slope's topography. First, in the case of a continuously moving deep-seated landslide, the time-dependent deformation itself can induce topographic changes, becoming more pronounced the longer the process continues. Typical resultant morphologies are a convex/bulge-shaped foot and a subsidence/concave-shaped middle and upper part (Agliardi et al., 2012; Zangerl et al., 2015). Second, spontaneous slope failure at the foot of such deep-seated slides becomes more likely the longer the slow deformation process lasts. Major mass relocation at the foot can have a significant impact on the superordinated sliding geometry, induce stress relocations and affect the deformation behaviour of the deep-seated landslide. Third, relocated material gets deposited in the valley and thus exposed to fluvial or torrential activity. Depending on local river characteristics, alluvial levels and associated buttressing effects can change over time and significantly affect the activity of deep-seated slides (Korup et al., 2010; Zangerl et al., 2015).

In order to assess topographic changes and consider them in a geomechanical model, topographic monitoring techniques as well as reconstruction and projection approaches were applied. Each topographic time step (see time series in Figure 2) became additionally parametrised by essential parameters comprising a geological model of the slope and respective geotechnical parameters. The geological model provides geometric information of lithological boundaries, sliding surface(s), slope topography and pore pressure distribution. In this study the internal friction angle (φ), cohesion (c), specific weight (γ) and the grain size distribution are used to describe the geomechanical characteristics of the sliding material. The applied modelling procedure focused on investigating the effect of changing boundary conditions or parameters (e.g., topography, pore water pressure distribution, cohesion, internal friction angle) on the stability and deformation behaviour of the Vögelsberg slope.

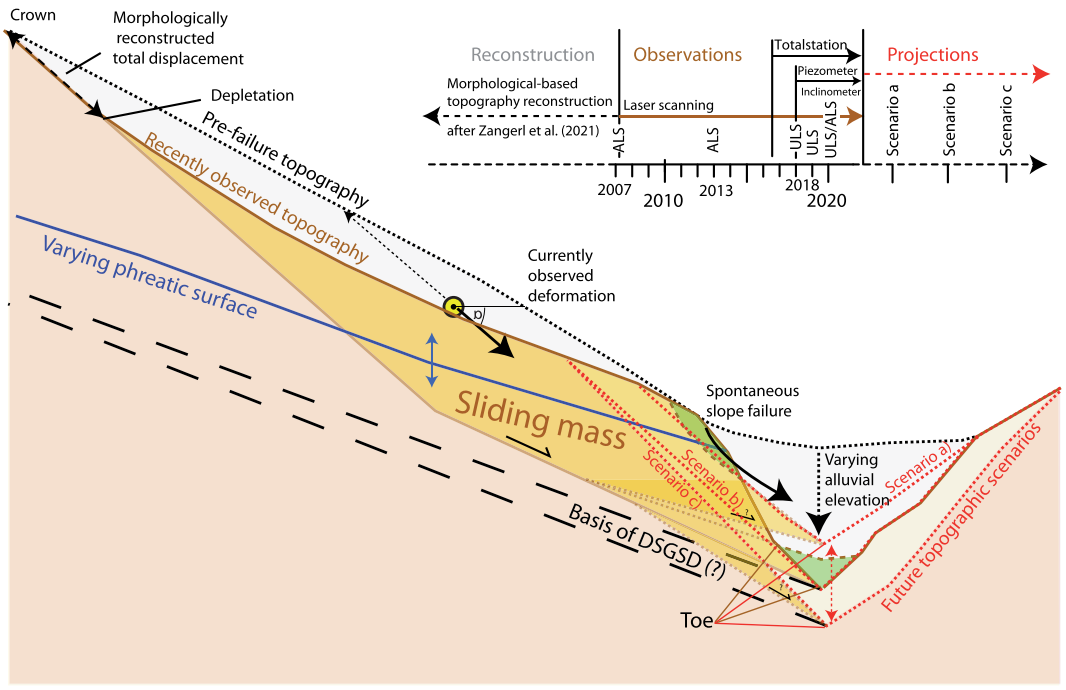

FIGURE 2 Research concept. Conceptual deep-seated landslide affected by hydrological and topographical changes potentially affecting a slope's stability. Schematic time series indicates datasets available for model parametrisation. Parametrisation beyond the observation period demand for reconstruction and projection approaches [Color figure can be viewed at wileyonlinelibrary.com]

3.2 | Subsurface monitoring

The subsurface of the active part of the landslide is investigated by a network of monitoring instruments in place since spring 2018. Knowledge about the subsurface is based on three core drillings (KB1, KB2 and KB3) conducted within the active landslide (Figure 1). Retrieved material samples were used for geotechnical characterisation of the sliding mass. Obtained cores were recorded and documented regarding their geological appearance (Engl, 2018). After core withdrawal, two boreholes (KB1 and KB2) were extended as groundwater monitoring wells continuously recording the piezometric head. One borehole (KB3) was equipped with an inclinometer. The screen of KB1 well was between 16 and 49 m depth, whereas KB2 was between 21 and 39 m below the surface. Periodic inclinometer measurements record the deformation pattern along a vertical profile and therefore provide information about the depth and range of current shearing. Coring and the installation of instruments were commissioned by the Austrian Service for Torrent and Avalanche Control.

3.3 | Monitoring the landslide's topography

ATTS measurements assess the 3D surface displacement at single points (retro-reflecting prisms) on a (sub)daily resolution. An ATTS installed on the opposite site of the Watten valley and operated by the federal state of Tyrol (division of geoinformation) performs position measurements of 53 ATTS retroreflecting prisms (Figure 3a). The measurements of each prism's 3D position results in a time series providing insights into the landslide-induced displacement at the respective location. Besides the derived 3D displacement vectors, the dense temporal resolution of these measurements enables a precise determination of the landslide's velocity, indicating phases of landslide acceleration or deceleration as a response to snowmelt or rainfall (Pfeiffer et al., 2021). The measurement accuracy is specified by the standard deviation of the decomposed time series ($\pm$ 0.54 cm a^{-1}).

In contrast to the ATTS measurements at single points, complementary laser scanning acquisitions provide an area-wide assessment of topography and landslide-induced surface changes (Hu et al., 2020; Pfeiffer et al., 2018). Three airborne laser scanning campaigns from October 2007, May 2013 and October 2020 were commissioned by the federal state of Tyrol and provide consistent 3D surface information of the study area. Three ULS campaigns were further carried out in 2018, 2019 and 2020 using a Riegl VUX-1LR laser scanner mounted on a Riegl RiCOPTER with an APPLANIX AP20 Inertial Measurement Unit (IMU) and two Sony Alpha 6000 digital cameras (Zieher et al., 2019). Efficient mission planning was carried out before acquisition using a simulation approach after Bremer et al. (2019) to fulfil flight security requirements, to optimise point densities and to ensure sufficient data coverage. The 3D point clouds were acquired in up to six individual flights per campaign, covering the Vögelsberg landslide, including areas surrounding the active part and the opposite site of the Watten valley to support multitemporal registration (Figure 3a). A pulse repetition rate (PRR) of 820 kHz, an angular step width of 0.06°, a beam divergence of 0.03°, a flight altitude between 50 and 60 m and a speed of approximately 8 m s^{-1} ensured a minimum point density of 500 points per square metre (Zieher et al., 2019). Specifications of utilised laser scanning data are summarised in Table 1. Multitemporal registration was carried out by applying the iterative closest point (ICP) algorithm (Besl & McKay, 1992) using stable areas (e.g., non-deformed or stable infrastructure, roads and buildings) within the point clouds. The point clouds were classified into ground and non-ground points using the TIN densification algorithm proposed by Axelsson (2000).

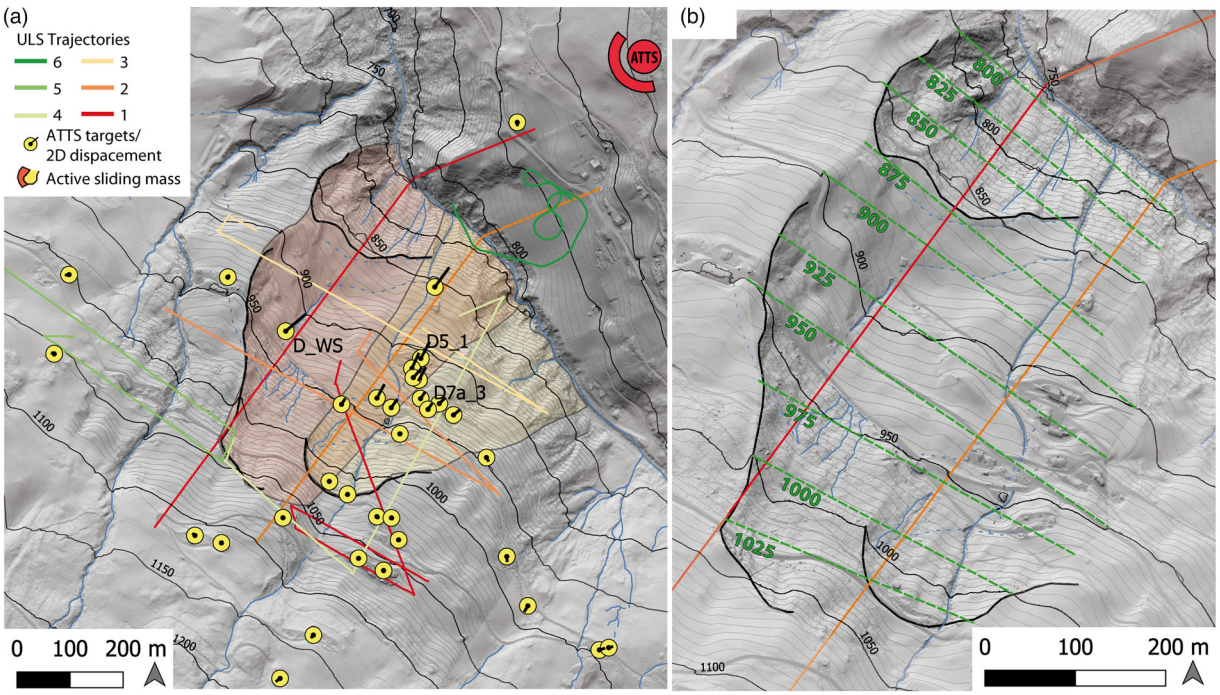

FIGURE 3 Panel (a) shows the topographic monitoring setup, ATTS position, prisms and respective 2D displacement vectors (1000-fold exaggerated). Panel (b) shows reconstructed contour lines (dashed green lines) following Zangerl et al. (2021), describing a probable pre-failure topography [Color figure can be viewed at wileyonlinelibrary.com]

TABLE 1 Characteristics of performed Laser scanning campaigns

Platform	Sensor	Date	Spatial resolution (cm)
ALS	ALTM 3100	13 Oct 2007	100
ALS	LMS-Q680i	18 May 2013	50
ULS	VUX-1LR	3 Aug 2018	2
ULS	VUX-1LR	14 Aug 2019	2
ALS	VQ-780 II	Oct/Nov 2020	50
ULS	VUX-1LR	6 Nov 2020	2

Digital terrain models with a spatial resolution of 0.25 m were derived from the classified ground points by aggregating the average elevation per raster cell. Digital terrain models of differences (DoD) were derived by subtracting subsequent multitemporal DTMs and used to assess topographic volumetric changes, which are particularly evident at the over-steepened foot due to secondary and spontaneous slope failures. For the area-wide assessment of coherent 3D displacements, an image correlation (IMCORR) approach that is able to assess vertical and horizontal displacement components was applied (Bremer, 2012; Fahnestock et al., 1992). For this analysis, hillshade images derived from the DTMs were used as input. In the next step, two selected cross-sections were extracted from the multitemporal point clouds in order to reconstruct a detailed surface representation for the slope stability analysis. Multitemporal profiles were further used (i) to assess recent incision or filling at the alluvium, (ii) to assess changes in the landslide's geometry due to secondary slope failures and (iii) as a basis to derive scenarios of potential future topographies.

3.4 | Reconstruction of past and scenario building of potential future topographies

A pre-failure topography was approximated using a reconstruction approach presented and applied to other deep-seated rockslides by Zangerl et al. (2015, 2021). This approach utilises present topographic information of assumed stable areas around the active and depressed sliding zone. Corresponding and hypothetical contour lines were mapped by inferring lines within the active, bowl-shaped and mass-depleted area (Figure 3b; Zangerl et al., 2021).

The plausibility of the reconstructed pre-failure topography was evaluated by re-transformation (rotation and translation) of a recent topographic profile (ALS 2007). Displacement vectors connecting corresponding points of the untransformed and the transformed part of the slope were compared to the observed ATTS displacement vectors along a 2D profile. Additionally, a morphologically based and reconstructed vector indicating the landslide's total experienced displacement was mapped by connecting the landslide's crown with the onset of its depletion zone (Figure 2). When the directional components of the recorded ATTS measurements and the morphologically reconstructed vector agree with the constructed vectors that are required to align present-day topography to the reconstructed pre-failure topography, the reconstruction approach is considered plausible.

Precisely assessed and quantified topographic changes by ALS and ULS over the last 13 years were the basis for the development of probable future topographic scenarios. Scenarios of spontaneous slope failures at the foot and related changes of the alluvial elevation were developed and their geomechanical effects on the Vögelsberg landslide were investigated. The first scenario represents a slope cross-section where the magnitude of observed slope failure and mass loss between 2007 and 2013 is tripled. Relocated material is deposited in the Watten River, inducing an elevation increase of approximately 25 m (Figure 4a). In a second scenario this material is assumed to be cleared by torrential or fluvial processes of the Watten River (Figure 4b). A third scenario is presumed as a continuation of river incision and describes a transect where the foot's upper topography is formed by the constructed slope failure from scenario 1, but the lower part of the foot is the result of further river incision (−25.5 m) and similar slope inclinations of the embankment as they are currently observed (Figure 4c). A fourth scenario consists of an ensemble of topographies and is based on the recent topography but step-wise investigates different alluvial elevations, deviating by +30 m to −30 m from the recent elevation level (Figure 4d).

3.5 | Geotechnical material characterisations

Material obtained from core drillings and representing the assumed shearing depth was analysed with regard to its grain size distribution, density (γ: specific weight) and shear parameter (φ: angle of internal friction and c: cohesion). Sieving and sedimentation tests were carried out to determine the grain size distributions of each sample per borehole. Immersion weighting was done with sealed and undisturbed samples to estimate the density. Five consolidated drained triaxial shear tests considering each of three different load steps (100, 200 and 300 kPa) with a shear velocity of 0.003 cm min^{-1} were carried out to assess the material's strength. Three disturbed samples (KB1, KB2 and KB3) were prepared in a 7 cm diameter cell. One additional sample obtained from KB3 was first prepared as an undisturbed sample and analysed in a 10 cm diameter cell applying a multi-step experiment. Subsequently, the same sample was re-prepared and investigated in a disturbed multi-step experiment in order to assess the potential effect of structures that could not be considered in disturbed samples. Table 2 summarises the installation properties of the samples analysed by triaxial shearing. The angle of internal friction and cohesion were analysed considering both the concepts of residual shear strength and peak shear strength.

3.6 | Geomechanical modelling: Slope stability assessment and model calibration

The analytical slope stability model GGU Stability (Bu, 2020) was used to calculate the balance of resisting and driving forces following the method of Janbu (1954) along a vertical 2D cross-section and for multiple observed, reconstructed and projected topographic and hydrological boundary conditions (Figure 5a). The resulting factor of safety (FoS) was used to determine the change of the slope's stability for different model parametrisations. Two vertical 2D cross-sections (Profile 1 and Profile 2; Figure 1a) following the slope inclination and intersecting with the boreholes were analysed. Supported by information deduced from the drilling cores' sequences, outcrops, field mapping,

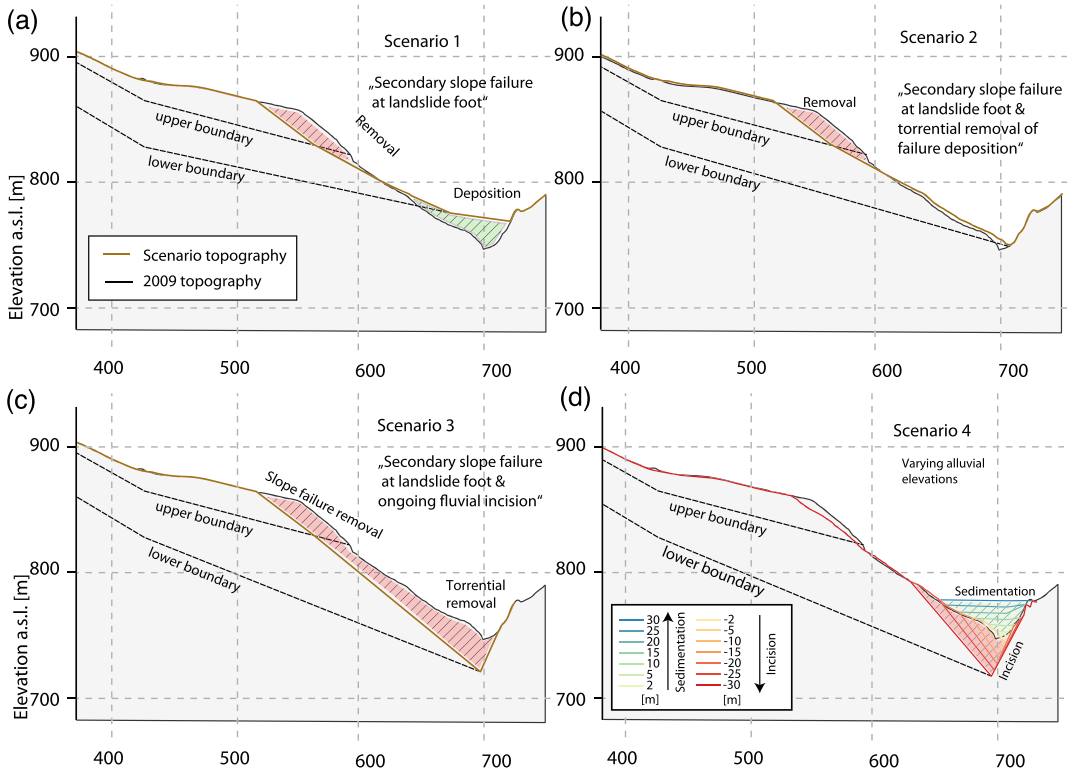

FIGURE 4 Topographic scenarios studied in the geomechanical model. (a) Scenario 1: severe secondary slope failure at over-steepened landslide foot. (b) Scenario 2: material deposited onto the river bed by Scenario 1 removed by fluvial river activity. (c) Scenario 3: ongoing fluvial incision. (d) Scenario 4: different alluvial elevations from 30 m sedimentation to −30 m incision [Color figure can be viewed at wileyonlinelibrary.com]

TABLE 2 Samples and their installation properties for triaxial shear tests

	KB1	KB2	KB3	$KB3_{undisturbed}$	$KB3_{disturbed}$
Extraction depth (m)	53	51	48	48	48
Cell diameter (cm)	7	7	7	10	10
Installation density (g cm^{-3})	2.2	2.2	2.1	2.3	2.3
Water content (%)	7.8	8.4	7.5	10.5	10.2

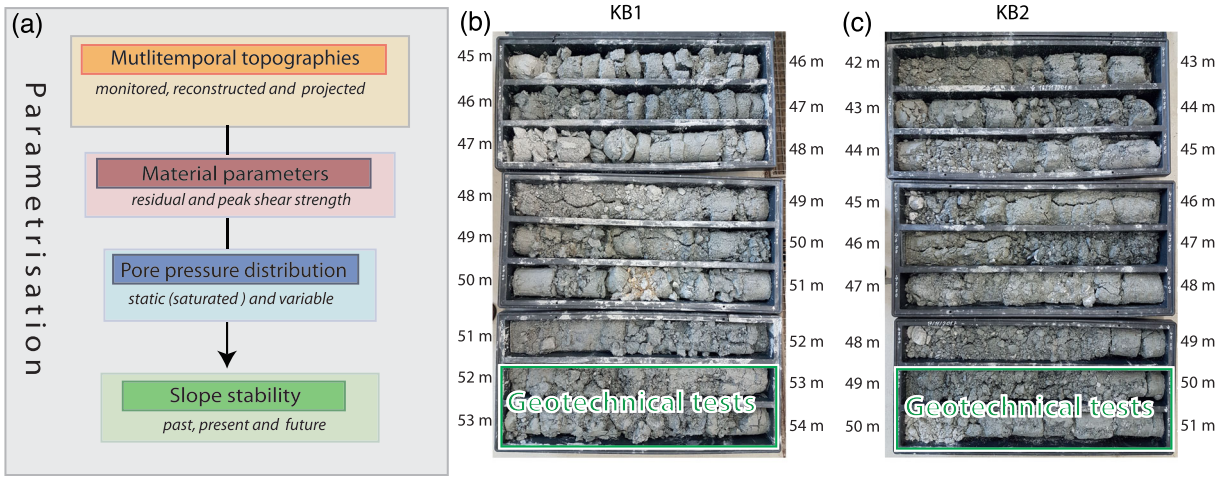

FIGURE 5 Workflow and photos of material samples. (a) Geomechanical modelling and parametrisation strategy able to assess the effect of long-term topographic and short-term hydrological changes. Photos of core drilling samples showing subsets in KB1 (b) from 45 to 54 m below the surface and in KB2 (c) from 42 to 51 m below the surface. Sections used for geomechanical material characterisation are indicated by a green polygon. Photos: J. Pfeiffer (08/2018) [Color figure can be viewed at wileyonlinelibrary.com]

piezometer records, inclinometer records and laser scanning data, two simplified geological models could be designed for use in the model.

Lower and upper boundaries defining the area of investigated slip surfaces were specified. Within this area possible slip surfaces were investigated and the one with the lowest FoS was kept as a result. The lower boundary of the investigated sliding mass was defined by the intersection point with the alluvial elevation (Watten River) at the landslide's toe, the bedrock depth within the boreholes and morphological indications for the onset of the depletion zone. The upper boundary was set in compliance with the requirement to allow only the formation of deep-seated sliding surfaces. A depth of 15 m below the surface for the central part was identified to be reasonable, neglecting the formation of small and shallow sliding surfaces, which were not the target of the investigation. Within this range all possible combinations of slip surface geometries were investigated. The slip surface indicating the lowest FoS (most unfavourable) was identified and compared to other results with different parametrisations.

Two definitions of pore pressure distributions were used within the modelling framework. For better comparability, the phreatic surface was set equal to the topographic line (saturated conditions) while modelling past, recent and future slope stabilities. In a separate model run, the effect of varying pore pressure distributions was investigated using present topographic conditions. Parametrised with recently observed piezometric heights and mapped spring districts, the effect of changing pore water distributions was investigated by various model runs and compared to corresponding deformation behaviour. The influence of a potential lowering of the phreatic surface induced by respective mitigation measures was additionally investigated by scenarios of lowered phreatic surfaces. Moreover, this model run aims at calibrating the model by identifying the parameter set that is close to the limit equilibrium of stability. On that basis a sensitivity analysis was performed by a systematic one-at-a-time (OAT) sensitivity analysis, since parameter sensitivity is variable among different landslides and depends on boundary conditions and geometry of the landslide (Schneider-Muntau et al., 2022).

4 | RESULTS

4.1 | Geological and geometrical landslide characterisation

Geomorphological mapping indicates a presence of two interacting slabs persistent at the active Vögelsberg landslide (Engl, 2018). Modelling Profile 2 passes the northwestern slab (Slab A) whereas modelling Profile 1 strikes along the intersection zone (Slab AB) of the southeastern Slab B and northwestern Slab A. The crown of Slab A is mapped at 1070 m a.s.l. Slab B's crown reaches maximum elevations of 1020 m a.s.l. The maximum elevation difference between Slab A's crown and the depletion zone is 103 m and shows a horizontal projected distance of 216 m. In movement direction this information is assumed to indicate the total experienced displacement of the active Vögelsberg landslide. Based on the mapped distances, the resulting displacement vector features a vertical angle of 25.5°, which agrees with the inclination of recently measured displacement vectors (see Section 4.2).

Consecutive inclinometer measurements performed in KB3 localise the deformation within −40 to −50 m depth below the surface. Within this range, most of the deformation focuses between −48 and −50 m (Figure 6c). Three core drillings revealed a sequence of disintegrated rock (i.e., soil) with depths of −53 m in KB2, −60 m in KB1 and −70 m in KB3 (Figure 5b,c; Engl, 2018). The volume of the disintegrated and loose rock mass is approximated by 10 million m^3 (Vecchiotti et al., 2022). Spring districts indicating intersection zones of groundwater and topography are tied to more inclined areas of the slope (Figures 1a and 6a,b), located right below the crown (920–1000 m a.s.l.) and at the over-steepened foot (800–850 m a.s.l.). Within the boreholes (KB1, KB2 and KB3) groundwater was encountered at −7.5, −4.2 and −24.2 m below the surface while drilling (Figure 6d; (Engl, 2018)). In KB2 the piezometric head varied between −8.5 and −7 m below the surface during the monitoring period from February 2018 to October 2021. The temporally varying movements observed at Slab A and the intersection zone (AB) show conformity with piezometer recordings in groundwater well KB2.The landslide's acceleration observed in spring 2019 coincided with periods of elevated phreatic level (Figure 6d)

Comparing the known characteristics of the landslide with criteria of the landslide classification scheme proposed by Cruden and Varnes (1996), the Vögelsberg landslide can be classified as an earth slide. Relevant key criteria are type of material and type of movement. The landslide material refers to earth since the moving mass consists of predominantly fine soil (see Section 4.3). The type of movement is defined as slide, since the transition from stable to moving along a vertical profile is observed to be within a relatively discrete zone of intense shear strain (Figure 6c; (Cruden & Varnes, 1996)). The high degree of disintegration of the sliding mass along the borehole indicates an intense history of shearing, which could be the result of multiple stress relocations and thereby induced relocations of shearing. Based on recent inclinometer measurements, the main shearing can be observed within a range of 2 m, which, compared to the thickness of 50 m of moving material in KB3, represents a small proportion. The applied geomechanical modelling approach therefore simplifies the shear zone to a single sliding plane. By transferring this geological knowledge onto the two modelling cross-sections (Profile 1 and Profile 2), the first step of geometrical model parametrisation was performed. Representing present topographic and hydrological conditions, these geometric models are applicable to the investigation of recent geomechanical characteristics (Figure 6a,b).

4.2 | Assessed, reconstructed and projected topographic changes

DoD maps indicate major erosion of about 18.400 m^3 material between 2007 and 2013 at the Vögelsberg landslides' foot, which occurred between 815 and 860 m a.s.l., covering an area of approximately 50 × 50 m and showing maximum erosion depths of up to −7 m (Figure 7a). Eroded material was deposited right below the removal zone at elevations between 815 and 740 m a.s.l. (Watten River), showing positive DoD map values in the range of 2–5 m. Maximum elevation gains of up to 7 m can be observed around the Watten River's alluvium. The volume of accumulated material is estimated as

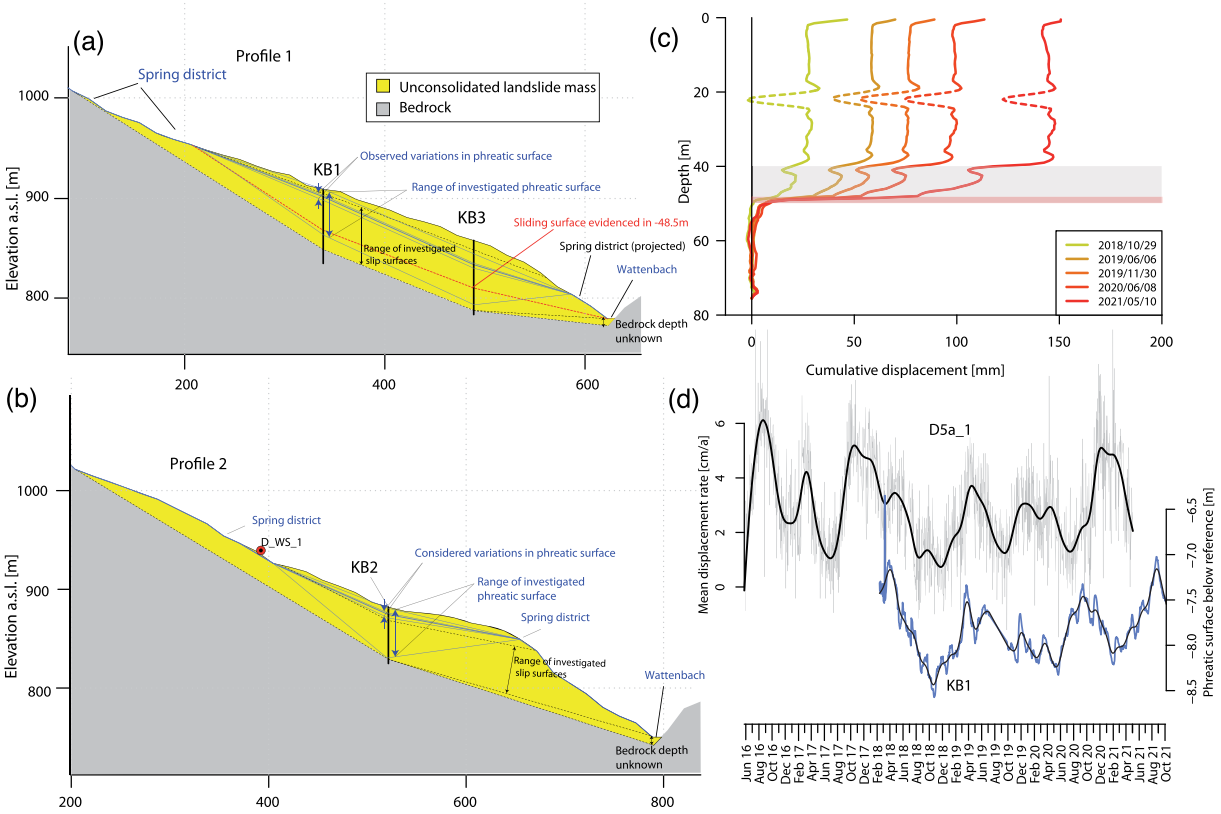

FIGURE 6 Geological models, inclinometer, piezometer and ATTS data. (a) Cross-section through KB1 drilling and (b) cross-section through KB2 and KB3 drillings integrated as reference in the geomechanical model; (c) depth profile of cumulative displacement assessed with repetitive inclinometer measurements and d) time series of landslide velocity (light grey: raw data; black: spline) and phreatic level (blue: raw data; black: spline) [Color figure can be viewed at wileyonlinelibrary.com]

16.500 m^3. This indicates a minor negative mass balance that could be associated with erosional effects of the Watten River.

7.400 m^3 of material was eroded between 2013 and 2020. The main erosion can be observed of the order of −2 to −3 m in height between 780 and 830 m a.s.l. (Figure 7b). Only a few raster cells within the DoD map represent positive values and therefore only a minor accumulation of 2.700 m^3, indicating a strongly negative mass balance. This observation points to the important role of the Watten River, which is assumed to remove relocated landslide material by torrential floods. In this context, well-recognisable erosion areas represented by negative DoD values of up to −2 m at the orographic left embankment indicate the destabilising effect of the Watten River.

Areas of coherent displacement could be identified based on the applied IMCORR algorithm between annual ULS acquisitions. The results reveal a distinct area of coherent 3D displacement with magnitudes of 3–4 m at the Vögelsberg landslide's foot between 780 and 815 m a.s.l. (Figure 7c,d). This area overlaps the erosion zone detected in the DoD map between 2013 and 2020. Areas of equidirectional displacement vectors indicate a highly active and pronounced sliding process which continuously changes the topography of the landslide's toe at considerably high movement rates. Compared to the general sliding of the deep-seated landslide of the order of 0.02–0.10 m a^{-1}, the intense displacements of multiple metres per year are attributed to shallower piggyback slides occurring on top of the Vögelsberg landslide's foot.

Whereas along modelling Profile 1 no significant topographic changes can be detected, modelling Profile 2 cuts these highly active area of piggyback slides and secondary spontaneous slope failures and visualises them along a cross-section (Figure 8a). The collapse of the foot between 2007 and 2013 and a distinct removal of material between 860 and 815 m a.s.l. reflected along the cross-section (Profile 2) is shown in Figure 8b. Relocated material was deposited in the Watten valley depression and temporarily induced a 3 m rise of the alluvial and an 8 m lateral shift of the river's position (Figure 8c). Between 2013 and 2020, 2 m incision of the river lowered the level of alluvium again. Material that accumulated at elevations between 815 and 750 m a.s.l. during the collapsing events of 2007–2013 was eroded between 2013 and 2020. In summary, the secondary (piggyback) slope failures that have occurred at the foot of Vögelsberg landslide have a considerable influence on the landslide's topography and are closely interlinked to the alluvial elevation. A decline of the landslide's mass as well as lateral and vertical shifts of the alluvium at the foot of the landslide are evident. Multitemporal laser scanning data demonstrates that significant topographic changes on the active landslide are associated with secondary slope failures at the foot and thereby the related rise of the alluvium (riverbed).

Reconstructed pre-failure topography, including extrapolated displacement vectors that are required to align pre-failure and present topography along the 2D cross-section, are shown in Figure 8d. The vertical component of the reconstructed vectors is within the range of vertical directions recently measured at ATTS prisms (Figure 9). The reconstructed topography overlays the current topography by up to 40 m and provides a considerably larger sliding mass before failure. Evidenced by the geomorphological shape and geometry of the

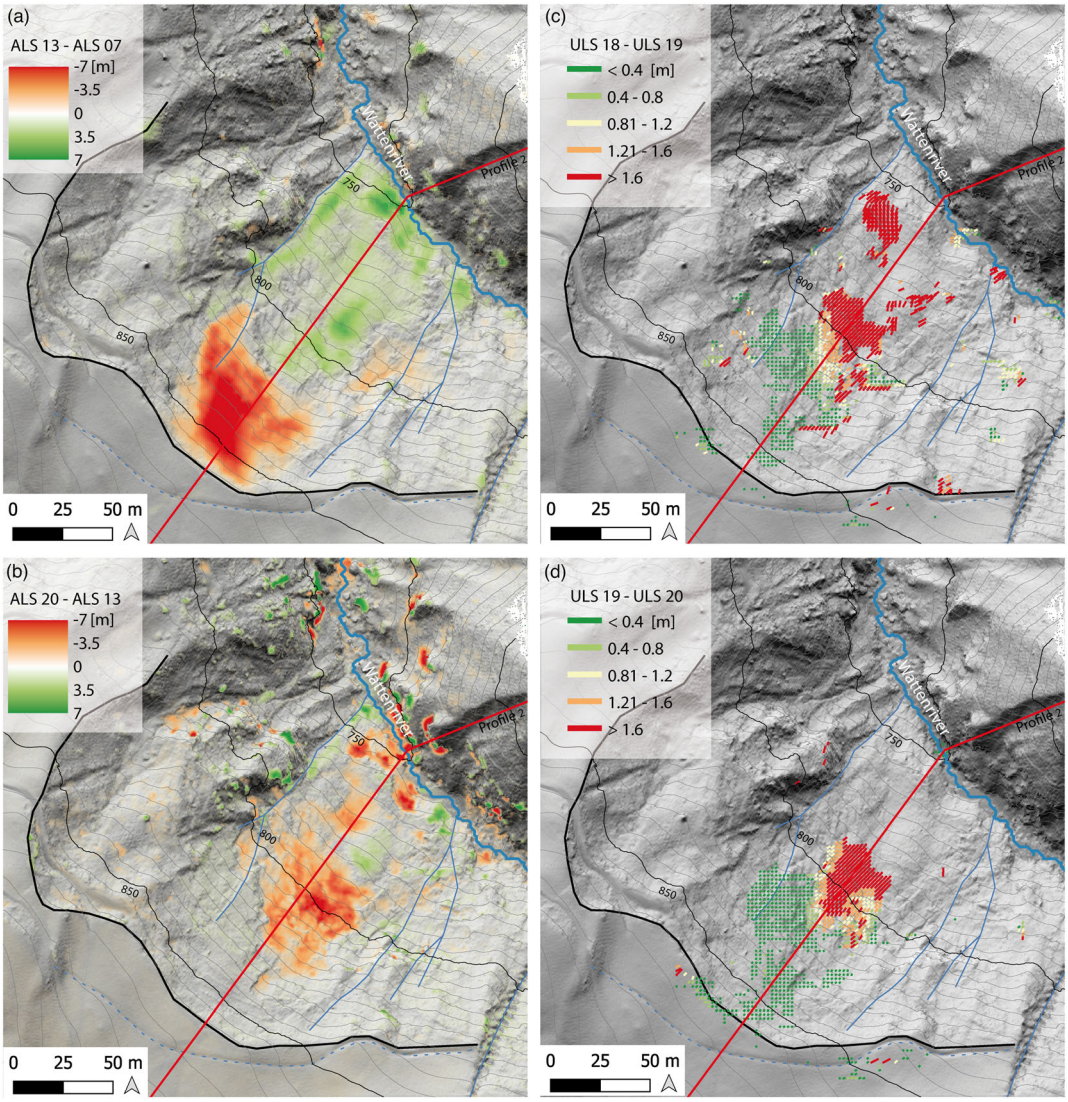

FIGURE 7 LiDAR-based maps of assessed topographic changes. Panels (a) and (b) show DoDs calculated by subtraction of ALS DTMs from 2007, 2013 and 2020. Negative values indicate mass loss and positive values indicate mass gain. Panels (c) and (d) show calculated annual 3D displacement vectors between the ULS acquisitions from 2018, 2019 and 2020 [Color figure can be viewed at wileyonlinelibrary.com]

Watten valley, a pronounced (post-glacial) fluvial overprinting of the glacially formed valley is obvious. Terraces located on the orographic right site of the Watten River are present at different elevations multiple tens of metres above the recent alluvium's height. Morphologically, these terraces could fit with the reconstructed pre-failure topography and entail the consideration of different alluvial heights while replicating and investigating the geomechanical formation of the Vögelsberg landslide. Therefore, topographic cross-sections including four different alluvial heights (+54, +3, +14 and ± 0 m) were combined with the landslide's pre-failure topography (Figure 8d). For the recent alluvium's elevation (± 0 m) additionally four embankment inclinations (70°, 40°, 35° and 30°) starting from the lowest point in the river were considered in individual model runs.

4.3 | Geotechnical parameter

The specific weight of the sliding mass material was determined between 20.3 and 21.2 kN m^{-3}. Supported by the observed continuous landslide deformation and indicated long history of deformation, the principle of residual shear strength (*r*0) was applied, assuming a cohesion of 0 kN m^{-2}. Analysing the peak shear strength (*peak*) indicates a cohesion between 0 and 38.4 kN m^{-2} and a friction angle between 26° and 32.6° valid for the analysed samples (Figure 10a and Table 3). Grain size distributions show well-graded, (extremely) poorly sorted and non-uniformly distributed characteristics and a clay content of less than 9% (10b).

4.4 | Slope stability

Under present conditions, results of geomechanical modelling indicate the slope to be either slightly above or slightly below its limit equilibrium, depending on the applied setting of material parameters, phreatic surface and the investigated cross-section. Resulting FoS calculated for each material parameter set (Table 3) and at static pore pressure distribution adapted to present observations are slightly above equilibrium limit. Differences can be observed between the two considered cross-sections. Profile 2 features generally lower FoS values compared to Profile 1 (Figure 11c). The OAT-sensitivity

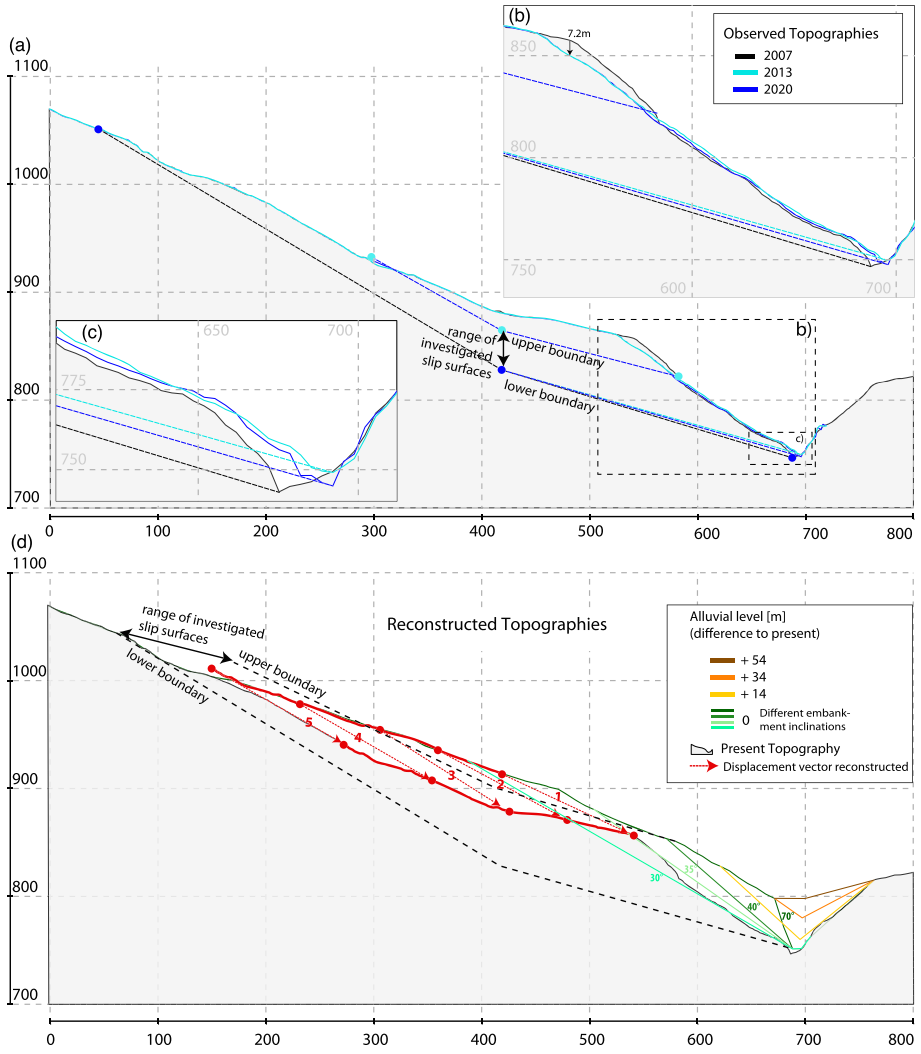

FIGURE 8 Multitemporal topographic 2D profiles used as input in the geomechanical model. Panel (a) shows observed multitemporal profiles from ALS data acquired in 2007, 2013 and 2020. Panel (b) highlights in more detail the topographic changes that occurred at the landslide foot and panel (c) stresses the changes that occurred at the river bed. Panel (d) shows different scenarios of topographies reconstructed after Zangerl et al. (2021), including different toe elevation and embankment inclinations. Red-dashed lines represent reconstructed displacement vectors (1–5) [Color figure can be viewed at wileyonlinelibrary.com]

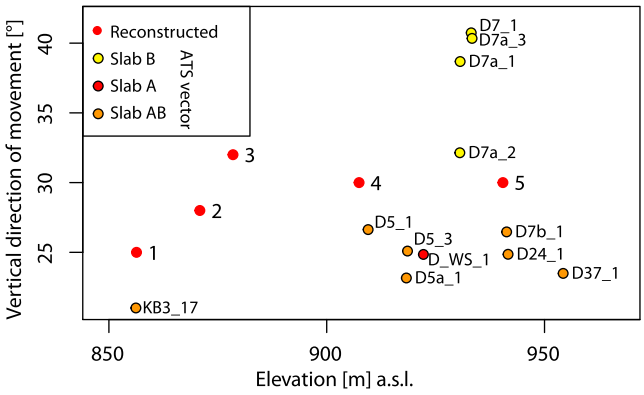

FIGURE 9 Inclination of the displacement of reconstructed (label: 1–5; see Figure 8b) and measured displacement vectors at their current elevation [Color figure can be viewed at wileyonlinelibrary.com]

analysis revealed the angle of internal friction and pore water distribution to be the most sensitive parameters tested at a constant predefined sliding geometry (Figure 12a). If higher values are adopted for the material parameters (φ, c and γ) the FoS enhances, implicating a more stable slope. The cohesion is observed to have the lowest sensitivity. Profile 2 is more sensitive to changes in the specific weight compared to Profile 1, where the sensitivity of specific weight and cohesion are almost equal. Nevertheless, the observed minor impact of varying cohesion values on the resulting slope stability should be evaluated differently when considering the concept of non-predefined sliding geometries. Material parameters can strongly influence the geometry of a failure mechanism (Schneider-Muntau et al., 2022). Investigations of different sliding geometries within a predefined range showed that the cohesion determines the depth of where sliding most likely occurs. Generally, the higher the cohesion the more likely it is that deeper and bent/slanted sliding surfaces developed.

Changes in material parameters (φ, c and γ) over time—for example, due to material disintegration—are neglected in this study and set to constant values for the landslide mass. This approach is valid, when considering residual strength parameters, which are not supposed to change due to further shearing. In contrast, hydrological conditions and topographic parameters were observed to change considerably over time. Among them, observed and projected short-term-variations in the phreatic surfaces show differences in sensitivity between the investigated cross-section. Profile 1 shows a more sensitive response to variations of phreatic surface compared to Profile 2. The 1.5 m range of observed phreatic variations between 2018 and 2021 induces a change in stability of 1.5% for Profile 1 and 1.1% for Profile 2 (Figure 12b). These variations in stability could be directly linked to recently observed variations in landslide velocity.

Between 2007 and 2020, significant topographic changes were assessed along Profile 2. Between the sub-period from 2007 to 2013,

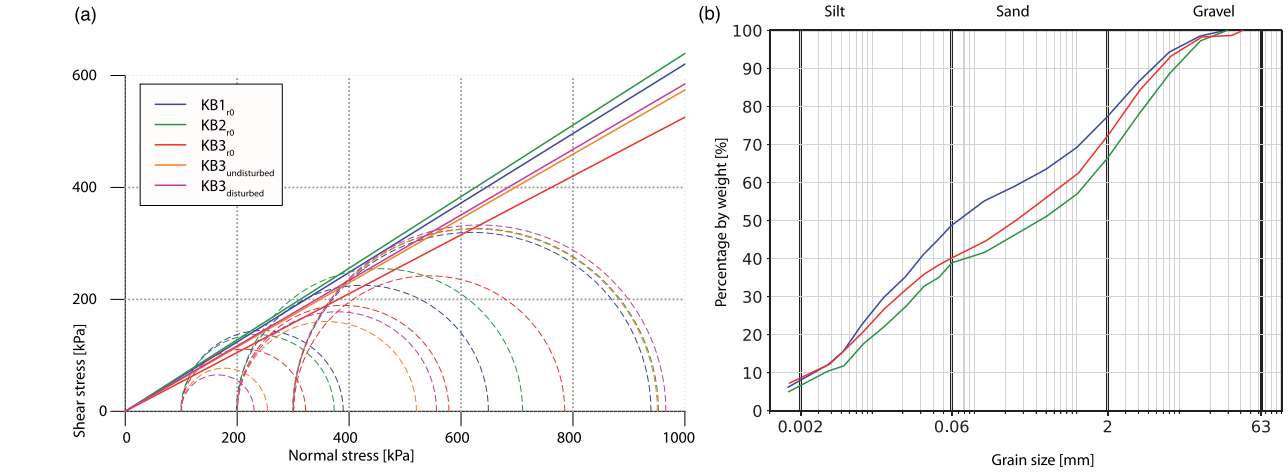

FIGURE 10 Geotechnical parameter: (a) triaxial shear test; (b) grain size distribution [Color figure can be viewed at wileyonlinelibrary.com]

TABLE 3 Geotechnical characteristics of the landslide mass

Sample	c_{peak}(kN m^{-2})	c_{r0}(kN m^{-2})	φ_{peak}(°)	φ_{r0}(°)	γ(kN m^{-3})
KB1	34.7	0	30.2	31.83	21.26
KB2	32.7	0	31.5	32.61	21.32
KB3	38.4	0	26	27.75	20.34
$KB3_{undisturbed}$	0	–	32.3	–	20.36
$KB3_{disturbed}$	9	–	31.4	–	20.59

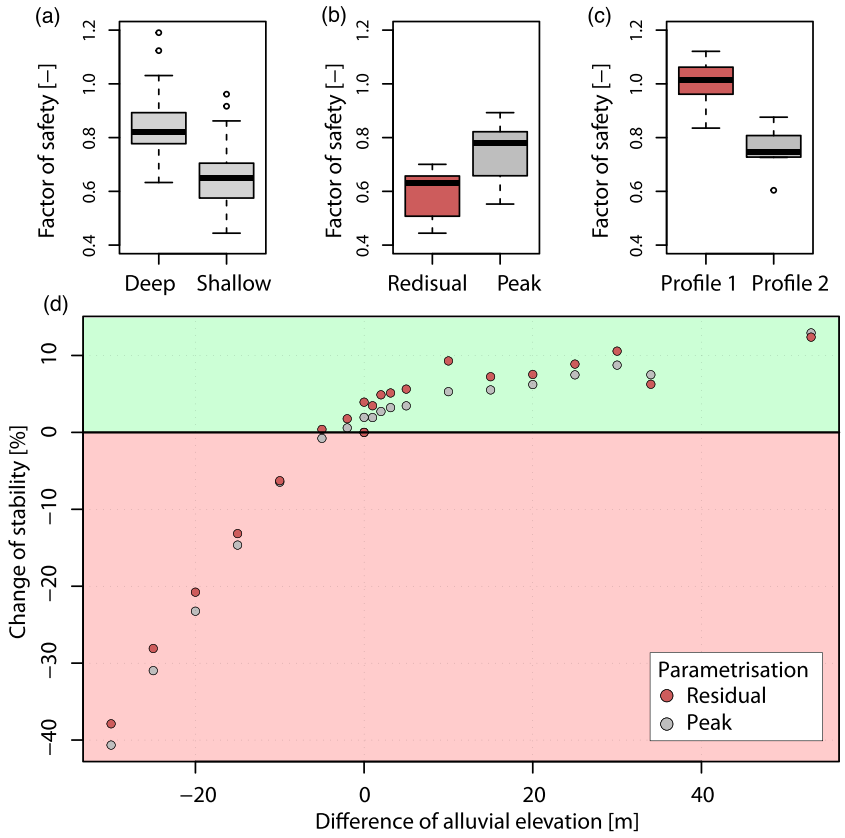

FIGURE 11 Resulting slope stability expressed by FoS and parametrised by a set of geotechnical parameters shown in Table 3. Boxplots (box: lower and upper quartile, whiskers: 1.5 * interquartile range) show differences between (a) deep (i.e., sliding surface close to lower boundary) or shallow (i.e., sliding surface close to upper boundary) sliding surfaces, (b) residual or peak parametrisation (only profile 2) and (c) the geometry of the modelled cross-section (Profile 1 vs. Profile 2). The lower graph (d) shows the effect of alluvial height deviations on changes in slope stability for a parametrisation using residual shear strength values ($\varphi = 32.6°$, $c = 0$ and $\gamma = 21.3$ kN m^{-3}) and peak shear strength values ($\varphi = 31.5°$, $c = 32.7$ kN m^{-2} and $\gamma = 21.3$ kN m^{-3}) [Color figure can be viewed at wileyonlinelibrary.com]

stability assessments for resulting model geometries yield a decrease in stability in the range of 5.1% for a residual shear strength parametrisation ($\varphi = 32.6°$, $c = 0$ and $\gamma = 21.3$ kN m^{-3}) and 3.2% for a peak shear strength parametrisation ($\varphi = 31.5°$, $c = 32.7$ kN m^{-2} and $\gamma = 21.3$ kN m^{-3}) (Figure 13). During the subsequent period from 2013 to 2020, resulting slope stability increases by 1.6% (residual) and 1.3% (peak), respectively. Considering the different alluvial elevations prevailing at respective investigated topographic

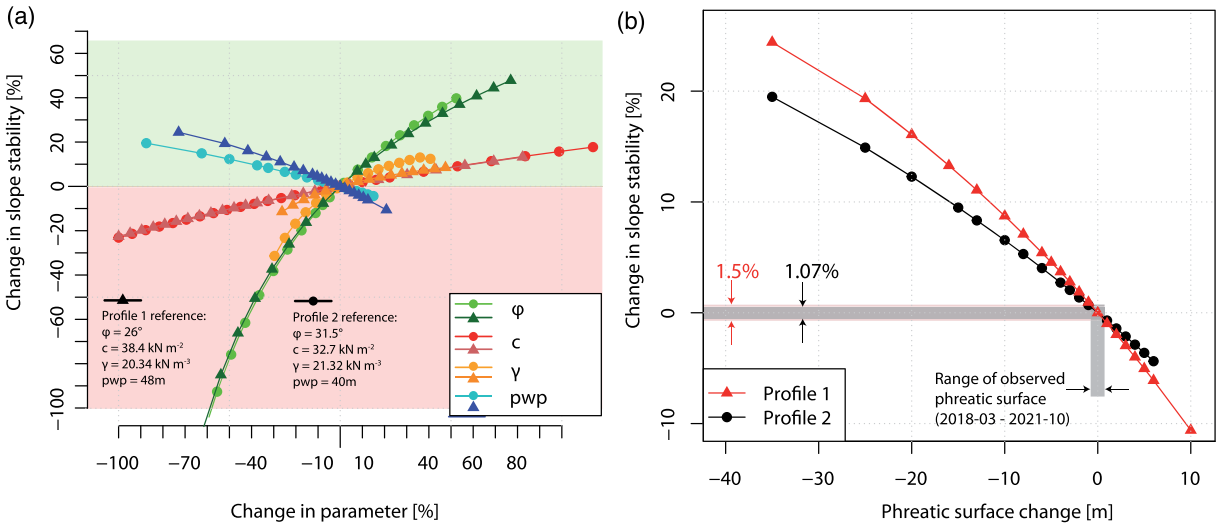

FIGURE 12 Parameter sensitivity. (a) Sensitivity of model parameters analysed by an OAT sensitivity analysis and (b) influence of groundwater level changes on the slope's stability [Color figure can be viewed at wileyonlinelibrary.com]

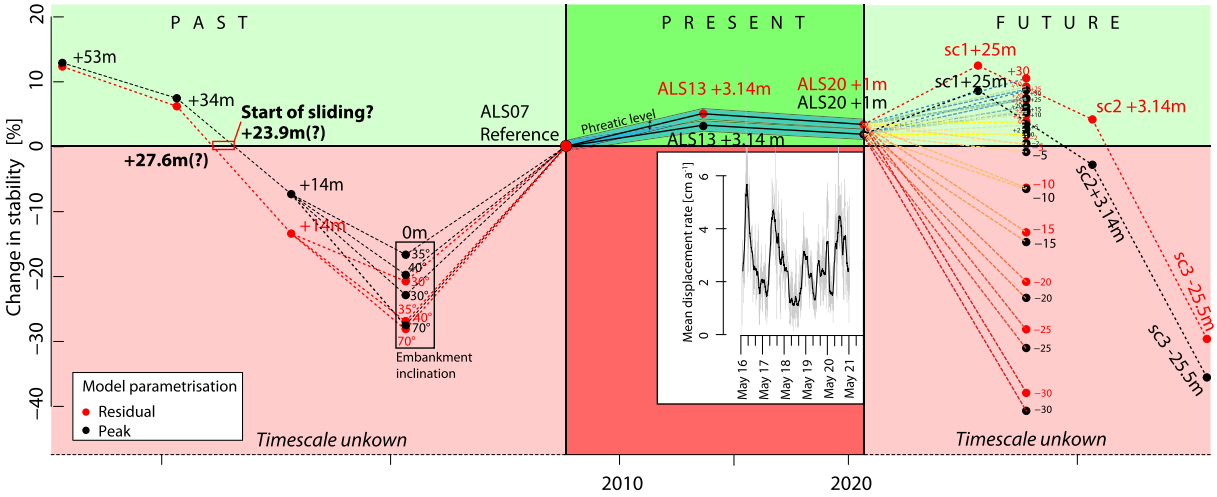

FIGURE 13 Effect of different topographies on the slope stability demonstrated at reconstructed past, observed present and projected future model geometries. Labels at data points refer to alluvial elevation deviations from the 2007 reference height. An overlain time series of displacement rate representing mean values of all ATTS reflectors within the unstable part shows short-term fluctuations of the landslide activity [Color figure can be viewed at wileyonlinelibrary.com]

parametrisation, it becomes obvious that alluvium uplift enhances stability and alluvial erosion reduces calculated stability. This nonlinear relation becomes even more pronounced while investigating the effects of reconstructed and projected topographic scenarios specifying a wide range of different alluvial levels (Figure 11d).

A hypothetical severe secondary slope failure event as represented by Scenario 1 would lead to an increased slope stability of +8.6% (residual) and +12.5% (peak). Potential future fluvial erosion to the alluvial level of 2020 (Scenario 2) would implicate equal stability conditions as they prevailed prior to Scenario 1. Continuous fluvial erosion as hypothetically pictured by Scenario 3 would negatively influence the stability (−35.5% for residual and −29.6% for peak shear strength) and therefore increase the activity of the Vögelsberg landslide. A distinct change in the sliding geometry is likely at an alluvial level between 5 and 10 m lower than the recent level (Figure 14). With increased lowering of the alluvium's level, a more frequent formation of shallower sliding surface (i.e., closer to the upper boundary of potential shearing) can be observed. Implications of potential future alluvial levels on the change in slope stability are shown in detail by results obtained from topographic ensembles investigated by Scenario 4. Starting from the present topography, a potential future increase in alluvial level of 35 m would increase the slope stability by +8.7% and +10.6%, respectively. An erosion of the same magnitude would, on the other hand, decrease the slope stability by −37.9% and −40.7%, respectively (Figure 13).

Assessed slope stabilities for the reconstructed pre-failure topographies are above the reference (ALS 2007) in the case that the assumed fluvial erosion has not reached an approximate level of 27.6 m and 23.9 m, respectively, above the current alluvium height. Further erosion leads to a pronounced stability decrease. The slope stability analysed using the pre-failure topography, the present alluvium level and an embankment of 70° indicate stability values of −28% below the topographic reference from 2007. Different embankment inclinations show additional influence on resulting change in stability. Whereas a steep inclined embankment features the most negative stability changes, less inclined embankments would

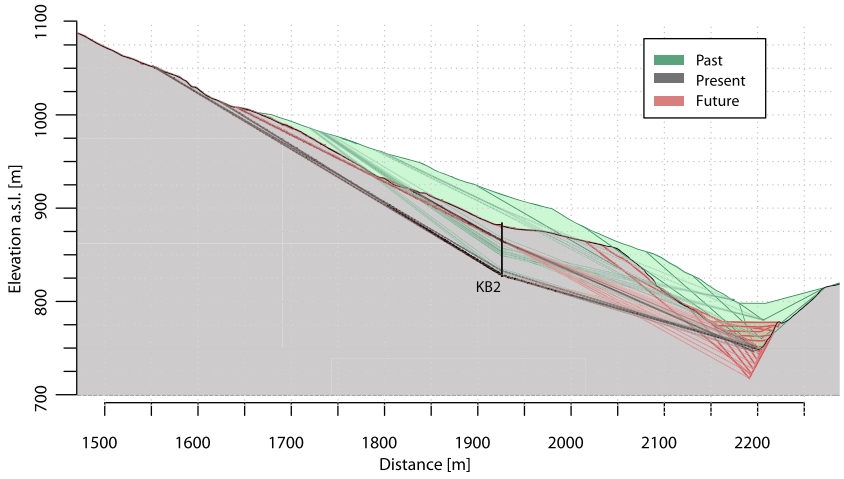

FIGURE 14 Investigated multitemporal topographies (reconstructed past, presently observed and future scenarios) along Profile 2 overlain by a compilation of resulting most unfavourable sliding surface (transparent lines) identified by geomechanical modelling [Color figure can be viewed at wileyonlinelibrary.com]

implicate comparably lower changes in stability (−20.7% for residual −22.8% for peak shear strength). Furthermore, it is observed that moderately inclined embankments tend to develop deep-seated sliding surfaces, whereas a steeply inclined embankment generally features more shallow sliding surfaces.

For the present and future topographic parametrisations, the material parameters referring to residual shear strength generally face higher slope stability changes compared to those derived by the peak shear strength parameters (Figures 11b and 13). Model runs parametrised with reconstructed topographies, on the other hand, show the opposite behaviour, which could be associated with sliding surfaces formed at different depths. Generally, stability values of sliding bodies where the most unfavourable sliding surface has formed at shallower areas (closer to the upper considered limit) are lower compared to those featuring a deep-seated sliding surface (closer to the lower considered limit) (Figure 11a). A compilation of identified, most unfavourable, sliding surfaces developed at past, present and future topographic parametrisations is shown in Figure 14, where the control of the alluvium level on the depth of the sliding surface is recognisable.

5 | DISCUSSION

The Vögelsberg landslide, a deep-seated earth slide located at the lower part of a large DSGSD, shows considerable deformation (2–10 cm a^{-1}), observed down to −50 m below the surface. An intense history of shearing, fragmentation and disintegration of bedrock formed the unconsolidated landslide mass, with the deepest known bedrock boundary at approximately 70 m below the surface. Detailed topographic monitoring based on ULS and ALS acquisitions have shown that parts of the over-steepened landslide foot were recently subjected to spontaneous slope failures and sliding processes exceeding magnitudes of 100 cm a^{-1}. Between 2007 to 2020 this mass relocation accounted for approximately 0.26% of the total estimated Vögelsberg landslide volume. Combined with fluvial and torrential activities, the alluvium level located at the landslide's foot was detected to be highly variable, experiencing vertical changes of the order of 3 m within 6 years. Even though point densities of classified ground points are typically low in forested and steep areas along the embankment of the Watten River, the magnitude of investigated topographic changes is multiple times higher compared to the spatial resolution of the data. Hence significant topographic changes could be assessed both along vertical cross-sections and area-wide. Topographic reconstruction and approximation of a pre-failure topography following Zangerl et al. (2021) revealed results that are consistent with currently observed displacement vectors. However, the reconstruction approach is straightforward, and the resulting topography must be considered a smoothed approximation of the pre-failure topography lacking topographic details (Zangerl et al., 2021). Furthermore, the interaction between DSGSD and therein hosted deep-seated landslide could not be considered due to unavailable information about DSGSD deformation potentially overprinting recent deformation and obtained results of the reconstructed pre-failure morphology of the Vögelsberg landslide.

Geomechanical analysis of driving and resisting forces of the Vögelsberg landslide has been shown to be close to limit equilibrium. The sliding mass defined in the cross-section through Slab A (Profile 2) is slightly dominated by driving forces, whereas along the intersecting Slab AB (Profile 1) resisting forces prevail. The generally higher velocity and the more pronounced temporal dynamics recorded on Slab A frame this model result. At constant topographic and material parameters, changes in the phreatic surface showing a range of 1.5 m are observed to control the landslide velocity. Starting from a reference parametrisation, observed hydrological variations were identified to affect the resulting slope stability by up to 1.5%. Correlations between recently recorded groundwater levels and displacement rates indicate modelled variations of slope stability to be reliable proxies for investigating the effects of potential future (e.g., measure-related) groundwater levels.

Assuming constant hydrological and material parameters, particularly the change in alluvium elevation, was identified to have the greatest influence on the slope's stability. Changes in topography therefore could affect the activity of the Vögelsberg landslide that would not be explainable by changes in the hydrological regime alone. A major increase in stability of the order of +3.2% (peak strength parametrisation) and +5.1% (residual strength parametrisation) is associated with secondary slope failures at the landslide's foot and the entailed uplift of the alluvium between 2007 and 2013. Whereas an uplift of the alluvium contributes to more stable conditions, removal of alluvium leads to a reduced stability of the slope. In absolute numbers, an alluvium rise of 1 m would induce an increase of stability by

0.7%. Potential future river incision, on the other hand, induces a slope stability decrease of the same magnitude until 5 m below the recent level. Between 10 and 30 m of incision, the gradient of stability decrease abruptly and rises to 1.6% per metre. Given that between 5 and 10 m of alluvium lowering a new, mostly unfavourable, sliding surface develops, this observation demonstrates the impact of differently shaped and inclined sliding geometries on potential erratic landslide behaviour.

Assessed stability variations attributed to topographic changes are representative of the investigated cross-section (Profile 2). Because the observed topographic changes are spatially restricted, presented values of topography-induced stability changes are assumed to constitute the upper of potential values. Observed secondary slope failures and thereby induced changes in the alluvium's level are limited to a 70 m lateral extent, which only represents a small proportion of the whole lateral extent of the Vögelsberg landslide (c. 350 m). Potentially stabilising 3D effects should therefore be considered while interpreting obtained results.

The bedrock depth is detected within three core drillings and assumed at outcrops around the landslide's scarp. Detailed evidence on the bedrock depth at the Watten River and geometric information about potential subsurface interactions between sliding mass and alluvial sediments is missing. Hence the range of investigated shear surfaces is fixed to the lowest potential slip surface, which is bound to the intersection with the profile's lower end (e.g., Watten River). However, Zangerl et al. (2015) obtained comparable results and proved the positive (e.g., buttressing) effect of the alluvium by using a 2D discrete element modelling approach that also takes account of subsurface interactions of a rockslide and alluvial deposits.

Strongly negative mass balances between present and reconstructed topographies indicate a long history of sliding. Initial formation of the deep-seated Vögelsberg landslide could be traced back to a post-glacial alluvium level of 23.9 m (peak strength) and 27.6 m (residual strength), resulting in limit equilibrium conditions. Investigated topographies featuring the reconstructed pre-failure surface but present-day alluvial levels indicate extraordinary and unlikely low FoS values and slope stability deviations of up to −28% below the reference of 2007. Although pre-failure conditions likely featured comparably higher material parameter values representing more stable conditions, these critical alluvial levels of between 23.9 and 27.6 m can be considered minimum values inferring landslide evolution. Assuming that present-day measured average velocities (5 cm a^{-1}) have prevailed since the formation of the Vögelsberg landslide and that the total experienced 3D displacement accounts for 240 m, a formation age of 4.8 ka before present could be estimated. Deceeding the limit equilibrium at the assumed critical alluvial level, simultaneous sliding and ongoing fluvial erosion are seen as interlinked dominant processes that led to today's topography. Although continuous and slow movement varies with a magnitude of several centimetres depending on the state of the hydrological forcing (Pfeiffer et al., 2021, 2022), its persistency throughout time is assumed to induce following process cascade. Preceding movements lead to recurring over-steepening of the foot, consecutive secondary slope failures spontaneously relocate material from the upper foot to the toe, and succeeding fluvial erosion removes temporarily deposited landslide material. Such a geomorphic feedback between landslides and river channels is well known from many tectonically active mountain belts (Korup et al., 2010).

Based on this, we conclude that recently observed short-term variations in landslide activity are directly associated with groundwater level variations. From a long-term perspective, recently explored effects of climate change on the activity of the Vögelsberg landslide indicate a reduced frequency of accelerating events (Zieher et al., 2022). On the other hand, topographic changes, in particular the interactions of the landslide foot with the Watten River's alluvium, are seen as a crucial variable regulating the landslide's response to adjustments of its geometrical boundaries.

6 | CONCLUSIONS

The present study investigates the effects of a changing topography on the stability of the slowly moving deep-seated Vögelsberg landslide in Tyrol (Austria). Observed topographic changes between 2007 and 2020 caused by rapid, secondary slope failures and piggyback slides at the foot of the landslide were included in the geomechanical modelling. For considering long-term changes of topography, the pre-failure topography was reconstructed based on geomorphological interpretation and by extrapolating today's observations of landslide velocity. Future scenarios of topography were then developed to assess the respective effects on the landslide's activity.

Besides of the hydrometeorological forcing, which is governing the landslide's seasonal and interannual dynamics, topographic changes modifying the sliding mass geometry were identified to have considerable impact on the location and form of the sliding surface and slope stability. On the one hand, mass relocation processes observed between 2007 and 2013 in the lower, over-steepened part of the landslide and the associated raise of the alluvium led to a general increase in slope stability. On the other hand, fluvial erosion successively deepened the alluvium between 2013 and 2020, causing a trend towards less stable conditions. These effects of present-day topographic changes on landslide activity are overprinted by dynamics of the hydrometeorological forcing, leading to variations in groundwater level, causing short-term stability changes.

Over longer time spans, landslide activity is governed by its geometry and the height of the alluvium (i.e., the valley bottom formed by the Watten River) as an interplay of sediment relocation at the over-steepened landslide foot and incision due to fluvial erosion. Based on the reconstructed pre-failure topography the onset of the landslide's movement was reanalysed and may have initiated when the alluvium reached 27.6 m above the recent level. Further scenarios considering various heights of the alluvium revealed that the landslide's activity may increase with progressing erosion by the Watten River. Furthermore, after the incision surpasses 5 m compared to today's level, the landslide may form a deeper sliding surface, potentially changing its behaviour fundamentally.

The presented modelling approach allows us to draw conclusions about the effects of mitigation measures. Changes in both the topography at the landslide's toe and the slope's hydrology are presumed to modify its activity pattern. Reducing the groundwater level may enhance slope stability by approximately 1% per metre. Raising the landslide's toe by, for example, enforced alluvial sedimentation enhances the stability by 0.7% per metre. Whenever

conclusions about topographic effects controlling the activity of deep-seated landslides are tainted by stabilising three-dimensional effects, the presented integrated topographic monitoring and geomechanical modelling approach is transferable to other case studies featuring similar data availability.

ACKNOWLEDGEMENTS

The present study was conducted within the OPERANDUM project. This project has received funding from the European Union's Horizon 2020 research and innovation programme under grant agreement No. 776848. We thank Magnus Bremer for acquiring and processing ULS data, Stefan Tilg for support in the geotechnical lab, Daniela Engl for fruitful in-depth discussions, the Federal State of Tyrol (Division of Geoinformation) for providing ALS and ATTS data and the Austrian Service for Torrent and Avalanche Control for providing piezometer and inclinometer data.

DATA AVAILABILITY STATEMENT

Data available on request from the authors.

ORCID

Jan Pfeiffer https://orcid.org/0000-0001-5352-6047
Barbara Schneider-Muntau https://orcid.org/0000-0001-5947-9181

REFERENCES

Agliardi, F., Crosta, G.B. & Frattini, P. (2012) Slow rock-slope deformation. In: Clague, J. J., Stead, D. (Eds) *Landslides: Types, mechanisms and modeling*. Cambridge University Press, pp. 207–221.

Agliardi, F., Crosta, G.B., Frattini, P. & Malus, M.G. (2013) Giant non-catastrophic landslides and the long-term exhumation of the european alps. *Earth and Planetary Science Letters*, 365, 263–274.

Ambrosi, C. & Crosta, G.B. (2006) Large sackung along major tectonic features in the central italian alps. *Engineering Geology*, 83(1-3), 183–200.

Axelsson, P. (2000) Dem generation from laser scanner data using adaptive tin models. *International Archives of Photogrammetry and Remote Sensing*, 33(4), 110–117.

Baltsavias, E.P. (1999) A comparison between photogrammetry and laser scanning. *ISPRS Journal of Photogrammetry and Remote Sensing*, 54(2), 83–94.

Besl, P.J. & McKay, N.D. (1992) A method for registration of 3-d shapes. *IEEE Transactions on Pattern Analysis and Machine Intelligence*, 14(2), 239–256.

Bonzanigo, L., Eberhardt, E. & Loew, S. (2007) Long-term investigation of a deep-seated creeping landslide in crystalline rock. part i. geological and hydromechanical factors controlling the campo vallemaggia landslide. *Canadian Geotechnical Journal*, 44(10), 1157–1180. https://doi.org/10.1139/T07-043

Brckl, E., Brunner, F.K. & Kraus, K. (2006) Kinematics of a deep-seated landslide derived from photogrammetric, GPS and geophysical data. *Engineering Geology*, 88(3-4), 149–159.

Bremer, M. (2012) Imcorr feature tracking. saga module reference. 2012. http://www.saga-gis.org

Bremer, M., Wichmann, V., Rutzinger, M., Zieher, T. & Pfeiffer, J. (2019) Simulating unmanned-aerial-vehicle based laser scanning data for efficient mission planning in complex terrain. *The International Archives of the Photogrammetry, Remote Sensing and Spatial Information Sciences* XLII-2/W13: 943–950.

Bu, J. (2020) Ggu-stability slope stability analysis and analysis of soil nailing and reinforced soil walls to din 4084 and ec 7. https://www.ggu-software.com/

Chigira, M. (1992) Long-term gravitational deformation of rocks by mass rock creep. *Engineering Geology*, 32(3), 157–184.

Corominas, J., Moya, J., Ledesma, A., Lloret, A. & Gili, J.A. (2005) Prediction of ground displacements and velocities from groundwater level changes at the vallcebre landslide (eastern pyrenees, spain). *Landslides*, 2(2), 83–96. https://doi.org/10.1007/s10346-005-0049-1

Crosta, G.B., Frattini, P. & Agliardi, F. (2013) Deep seated gravitational slope deformations in the european alps. *Tectonophysics*, 605, 13–33. Slope Tectonics: Structures and Slope Failures.

Cruden, D.M. & Varnes, D.J. (1996) Landslide types and processes. In: Turner, A. K. & Schuster, R. L. (Eds) *Landslides: investigation and mitigation*, Vol. 247. Transportation Research Board Special Report 247, National Research Council, USA, pp. 36–75.

Eberhardt, E. (2008) Twenty-ninth canadian geotechnical colloquium: The role of advanced numerical methods and geotechnical field measurements in understanding complex deep-seated rock slope failure mechanisms. *Canadian Geotechnical Journal*, 45(4), 484–510. https://doi.org/10.1139/T07-116

Eberhardt, E., Bonzanigo, L. & Loew, S. (2007) Long-term investigation of a deep-seated creeping landslide in crystalline rock. part ii. mitigation measures and numerical modelling of deep drainage at campo vallemaggia. *Canadian Geotechnical Journal*, 44(10), 1181–1199. https://doi.org/10.1139/T07-044

Engl, D. (2018) Bericht aktueller kenntnisstand hangbewegung gelsberg gde. wattens, Forsttechnischer Dienst für Wildbach- und Lawinenverbauung.

Fahnestock, M.A., Scambos, T.A. & Bindschadler, R.A. (1992) Semi-Automated Ice Velocity Determination from Satellite Imagery. *Eos Transactions AGU*, 73, 493.

Gigli, G., Morelli, S., Fornera, S. & Casagli, N. (2014) Terrestrial laser scanner and geomechanical surveys for the rapid evaluation of rock fall susceptibility scenarios. *Landslides*, 11(1), 1–14. https://doi.org/10.1007/s10346-012-0374-0

Glueer, F., Loew, S., Manconi, A. & Aaron, J. (2019) From toppling to sliding: Progressive evolution of the moosfluh landslide, switzerland. *Journal of Geophysical Research: Earth Surface*, 124(12), 2899–2919. https://doi.org/10.1029/2019JF005019

Grafenauer, J. (2014) Geologische kartierung und numerische modellierung der gleitung wattenbach/eggerbach. Master's Thesis, Institut 474 für angewandte Geologie, Department für Bautechnik und Naturgefahren, Universität für BodenkulturWien.

Haditsch, J.G. & Mostler, H. (1983) The succession of ore mineralization of the lower austroalpine innsbruck quartzphyllite. In: Schneider, H.-J. (Ed) *Mineral deposits of the alps and of the alpine epoch in europe*. Berlin, Heidelberg: Springer Berlin Heidelberg, pp. 51–59.

Hofmann, R. & Sausgruber, J.T. (2017) Creep behaviour and remediation concept for a deep-seated landslide, navistal, tyrol, austria. *Geomechanics and Tunnelling*, 10(1), 59–73. https://doi.org/10.1002/geot.201600066

Hu, X., Brgmann, R., Schulz, W.H. & Fielding, E.J. (2020) Four-dimensional surface motions of the slumgullion landslide and quantification of hydrometeorological forcing. *Nature Communications*, 11(1), 2792. https://doi.org/10.1038/s41467-020-16617-7

Jaboyedoff, M., Oppikofer, T., Abelln, A., Derron, M.-H., Loye, A., Metzger, R. & Pedrazzini, A. (2012) Use of lidar in landslide investigations: a review. *Natural Hazards*, 61(1), 5–28. https://doi.org/10.1007/s11069-010-9634-2

Janbu, N. (1954) Application of composite slip surface for stability analysis, Proceedings of european conference on stability of earth slopes, sweden, 1954, Vol. 3.

Klebinder, K. & Graf, A. (2012) Monitoring massenbewegung wattenbach/eggerbachv gelsberg, gemeinde wattens, Bundesforschungszentrum für Wald (BFW).

Korup, O., Densmore, A.L. & Schlunegger, F. (2010) The role of landslides in mountain range evolution. *Geomorphology*, 120(1), 77–90.

Lacroix, P., Handwerger, A.L. & Bièvre, G. (2020) Life and death of slow-moving landslides. *Nature Reviews Earth & Environment*, 1(8), 404–419.

Molnar, P. (2004) Interactions among topographically induced elastic stress, static fatigue, and valley incision. *Journal of Geophysical Research*, 109, F2. https://doi.org/10.1029/2003JF000097

Patzelt, G. (1987) Untersuchungen zur nacheiszeitlichen schwemmkegel- und talentwicklung in tirol. *Veröffent. Mus. Ferd*, 67, 93–123.

Pfeiffer, J., Zieher, T., Bremer, M., Wichmann, V. & Rutzinger, M. (2018) Derivation of three-dimensional displacement vectors from multi-temporal long-range terrestrial laser scanning at the reissenschuh landslide (tyrol, austria). *Remote Sensing*, 10(11), 1688. https://doi.org/10.3390/rs10111688

Pfeiffer, J., Zieher, T., Schmieder, J., Bogaard, T., Rutzinger, M. & Spötl, C. (2022) Spatial assessment of probable recharge areas – investigating the hydrogeological controls of an active deep-seated gravitational slope deformation. *Natural Hazards and Earth System Sciences*, 22(7), 2219–2237.

Pfeiffer, J., Zieher, T., Schmieder, J., Rutzinger, M. & Strasser, U. (2021) Spatio-temporal assessment of the hydrological drivers of an active deep-seated gravitational slope deformation: The vögelsberg landslide in tyrol (austria). *Earth Surface Processes and Landforms*, 46(10), 1865–1881. https://doi.org/10.1002/esp.5129

Preisig, G. (2020) Forecasting the long-term activity of deep-seated landslides via groundwater flow and slope stability modelling. *Landslides*, 17(7), 1693–1702. https://doi.org/10.1007/s10346-020-01427-1

Preisig, G., Eberhardt, E., Smithyman, M., Preh, A. & Bonzanigo, L. (2016) Hydromechanical rock mass fatigue in deep-seated landslides accompanying seasonal variations in pore pressures. *Rock Mechanics and Rock Engineering*, 49(6), 2333–2351. https://doi.org/10.1007/s00603-016-0912-5

Rockenschaub, M., Kolenprat, B. & Nowotny, A. (2003) Innsbrucker quarzphyllitkomplex, tarntaler mesozoikum, patscherkofelkristallin, Geologische Bundesanstalt - Arbeitstagung 2003: Blatt 148 Brenner.

Salvini, R., Francioni, M., Riccucci, S., Bonciani, F. & Callegari, I. (2013) Photogrammetry and laser scanning for analyzing slope stability and rock fall runout along the domodossola iselle railway, the italian alps. *Geomorphology*, 185, 110–122.

Scaioni, M., Longoni, L., Melillo, V. & Papini, M. (2014) Remote sensing for landslide investigations: An overview of recent achievements and perspectives. *Remote Sensing*, 6(10), 9600–9652.

Schneider-Muntau, B., Dai, X. & Fellin, W. (2022) Sensitivity analyses of the different influencing factors on numerical investigations of landslides. *Geomechanics and Tunnelling*, 15(5), 582–595. https://doi.org/10.1002/geot.202200014

Tofani, V., Segoni, S., Agostini, A., Catani, F. & Casagli, N. (2013) Technical note: Use of remote sensing for landslide studies in europe. *Natural Hazards and Earth System Sciences*, 13(2), 299–309.

Van Asch, T.W.J. & Buma, J.T. (1997) Modelling groundwater fluctuations and the frequency of movement of a landslide in the terres noires region of barcellonnette (france). *Earth Surface Processes and Landforms*, 22(2), 131–141.

Vecchiotti, F., Amabile, A.S., Clemente, S., Ostermann, M., Nicodemo, G. & Peduto, D. (2022) Kinematic and geometric characterization of the gelsberg rockslide (tyrol, austria) by means of mt-insar data. *Geosciences*, 12(7), 256.

Zangerl, C., Chwatal, W. & Kirschner, H. (2015) Formation processes, geomechanical characterisation and buttressing effects at the toe of deep-seated rock slides in foliated metamorphic rock. *Geomorphology*, 243, 51–64.

Zangerl, C., Eberhardt, E. & Perzlmaier, S. (2010) Kinematic behaviour and velocity characteristics of a complex deep-seated crystalline rockslide system in relation to its interaction with a dam reservoir. *Engineering Geology*, 112(1), 53–67.

Zangerl, C., Schneeberger, A., Steiner, G. & Mergili, M. (2021) Geographic-information-system-based topographic reconstruction and geomechanical modelling of the köfels rockslide. *Natural Hazards and Earth System Sciences*, 21(8), 2461–2483.

Zieher, T., Bremer, M., Rutzinger, M., Pfeiffer, J., Fritzmann, P. & Wichmann, V. (2019) Assessment of landslide-induced displacement and deformation of above-ground objects using uav-borne and airborne laser scanning data. *ISPRS Annals of the Photogrammetry, Remote Sensing and Spatial Information Sciences* IV-2/W5, 461–467.

Zieher, T., Gallotti, G., Rianna, G., Reder, A. & Pfeiffer, J. (2022) Exploring the effects of climate change on the water balance of a continuously moving deep-seated landslide. *Natural Hazards*. https://doi.org/10.1007/s11069-022-05558-7

How to cite this article: Pfeiffer, J., Zieher, T. & Schneider-Muntau, B. (2023) Slope stability evolution of a deep-seated landslide considering a constantly deforming topography. *Earth Surface Processes and Landforms*, 48(5), 923–939. Available from: https://doi.org/10.1002/esp.5527